ISSN: 0976-9102 (ONLINE)
DOI: 10.21917/ijivp.2016.0195

ANALYSIS OF ABNORMALITIES IN COMMON CAROTID ARTERY IMAGES USING MULTIWAVELETS

R. Nandakumar[1] and K.B. Jayanthi[2]
[1]*Department of Electronics and Communication Engineering, K.S.R. Institute for Engineering and Technology, India*
E-mail: [1]nandhu.r79@gmail.com
[2]*Department of Electronics and Communication Engineering, K.S. Rangasamy College of Technology, India*
E-mail: [2]jayanthikb@gmail.com

Abstract

According to the report given by World Health Organization, by 2030 almost 23.6 million people will die from cardiovascular diseases (CVD), mostly from heart disease and stroke. The main objective of this work is to develop a classifier for the diagnosis of abnormal Common Carotid Arteries (CCA). This paper proposes a new approach for the analysis of abnormalities in longitudinal B-mode ultrasound CCA images using multiwavelets. Analysis is done using HM and GHM multiwavelets at various levels of decomposition. Energy values of the coefficients of approximation, horizontal, vertical and diagonal details are calculated and plotted for different levels. Plots of energy values show high correlation with the abnormalities of CCA and offer the possibility of improved diagnosis of CVD. It is clear that the energy values can be used as an index of individual atherosclerosis and to develop a cost effective system for cardiovascular risk assessment at an early stage.

Keywords:

Ultrasound, Common Carotid Artery, Multiwavelets, Energy Measurement, Classification

1. INTRODUCTION

For screening the cardiovascular diseases of the carotid artery, ultrasound imaging is a common procedure as the vessel is easily accessible with ultrasound probes [1]. Because of CVDs more people die annually than from any other cause. It has been reported by World Health Organization in a recent study that in the year 2008 nearly 17.3 million people died from CVDs. This represents 30% of all global deaths. In this 7.3 million people died due to coronary heart disease and 6.2 million were due to stroke [2].

Arteries are blood vessels that carry blood between the heart, different tissues and organs of the body. They have ability to expand or contract to allow more blood or control the flow. Hollow centre through which blood flows is called lumen. CCA supplies oxygenated blood to skull, brain, eyeballs, ears and external nose [3]. When the blood supply to parts of the brain is suddenly interrupted, stroke occurs. Aortic stiffness has been proven to be a strong independent predictor of all-cause and CVD. Estimation of regional stiffness of the carotid artery is of great clinical interest [4]. The changes in stiffness with age are accelerated in hypertension and highly amplified by the association with other CVDs and concomitant risk factors [5].

Atherosclerosis is the thickening and narrowing of the arteries due to formation of plaque on the walls of the artery. It causes enlargement of the arteries and thickening of the artery walls [6, 7]. The diameter of CCA decreases due to increase in the thickness. This causes a reduction of the lumen with possible vascular problems and alters the arterial properties elasticity and stiffness. Precise segmentation of carotid artery allows the computation of various biomechanical and anatomical properties of the artery wall that may be useful to clinicians to follow the evolution of the atherosclerosis diseases [8].

Ultrasound imaging has the advantage that it is noninvasive and does not involve the use of ionizing radiation. It is therefore ideally suited to serial investigations. It is also relatively inexpensive and images are acquired in real time [9, 10]. Longitudinal B-mode ultrasound images are used in this work. The resolution of diagnostic ultrasound image is significantly limited by speckle noise. It is believed that speckle is a high frequency component of the image [11]. As the texture of speckle often carries useful information, it is not truly a noise in the typical engineering sense. Ultrasound experts with insufficient experience may not often draw useful conclusions from the images due to the presence of speckle.

Though different methods are investigated for the analysis of carotid artery, the need still exists for the development, implementation and evaluation of an integrated system enabling the automated diagnosis. In the previous work boundary of CCA was extracted using watershed and wavelet transforms. The diameter was measured from the extracted boundary and used for the analysis of plaque deposit in the vessel [12][13]. In this work an effort is made to analyse the CCA using multiwavelets and correlate the findings with the atherosclerosis.

Multi scale representation has proven to be useful in many image processing applications. Recently, multiwavelets have been introduced as a more powerful multi-scale analysis tool. A scalar wavelet system is based on a single scaling function and mother wavelet. But multiwavelet system is based on several scaling functions and mother wavelets. It has several useful properties such as symmetry, orthogonality, short support and a higher number of vanishing moments simultaneously [14].

Multiwavelets can simultaneously provide perfect reconstruction, while preserving length (orthogonality), good performance at the boundary (via linear phase symmetry) and a higher order of approximation (vanishing moments). These features of multiwavelets are responsible for the better performance of multiwavelets over scalar wavelets in image processing applications [15,16]. Geronimo, Hardin and Massopust constructed one of the most well-known multiwavelets called GHM. GHM basis provides a combination of orthogonality, symmetry and compact support that is unachievable by any other scalar wavelet basis [17]. HM and GHM multiwavelets are used in this work to analyse the normal and abnormal CCA images.

2. MATERIALS AND METHODS

2.1 IMAGE ACQUISITION AND DATABASE

A group of 104 normal and abnormal subjects are used in this study. The arterial movements are recorded in the ultrasound machine. Value of the ultrasound scanner settings is an important issue affecting reliable recording of sequences of images. Appearance of anatomical structures and therefore the interpretation of the resulting images may be affected due to wrong settings. The probe used is a multi-frequency probe of range 5-10 MHz. For this application the frequency is set at 7.5 MHz, since the CCA is at an optimum distance from the skin. The video is recorded for 2 to 3 cardiac cycles showing the longitudinal view of the CCA in B-mode at a rate of 29 frames per second. The blood pressure of the patient is also checked and recorded. The video clipping is first cut into frames and stored in a file ready for processing.

2.2 LAYERS OF CCA

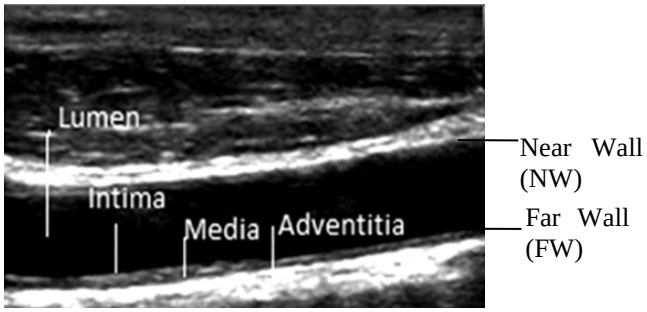

Fig.1. Longitudinal view of CCA

A sample image showing the longitudinal view of CCA is given in Fig.1. The artery wall consists of three layers. The outermost is called adventitia, the middle media and the innermost intima. In longitudinal view, the CCA is seen as a dark region comprised of lumen between the near walls (NW) and far walls (FW). Because of the poor difference in the acoustic impedance of the two adjacent layers, the intima layer is poorly represented. It is fused with the media layer. A dark grey is used to represent the media layer, whereas the adventitia layer appears as a bright grey and it is highly echogenic. The distance between the Lumen-Intima (LI) and the Media-Adventitia (MA) boundaries is called IMT. Usually plaque is formed on the intima layer and narrows the lumen.

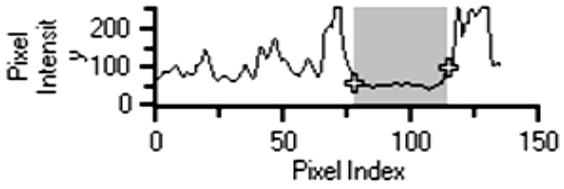

Fig.2. Intensity profile

The intensity profile along the vertical axis is shown in the Fig.2. Pixel values within the boundary of lumen are shown as shaded area in the profile. Formation of plaque alters the boundary of lumen. The multiwavelet preserves high frequency information in the image i.e. in boundaries. As the symmetric property of multiwavelets is very useful when dealing with image boundaries and prevents discontinuity at the boundaries and loss of information, abnormalities in CCA due to the formation of plaque can be correlated to the energy values of subbands obtained by multiwavelet decomposition.

2.3 MULTIWAVELET TRANSFORM

Multiscaling function vector $\Phi(x)$ and Multiwavelet function vector $\Psi(x)$ are used in the multiwavelet system [18][19].

$$\Phi(x) = (\phi_1, \phi_2,...,\phi_r)^T \quad (1)$$

$$(x) = (\psi_1, \psi_2,...,\psi_r)^T \quad (2)$$

which satisfies the following two scale relations.

$$\Phi(x) = \sqrt{2}\sum_{k\in Z} H_k \phi_k(2x-k) \quad (3)$$

$$(x) = \sqrt{2}\sum_{k\in Z} G_k \phi_k(2x-k) \quad (4)$$

The norm of the r scaling functions is maintained by $\sqrt{2}$ with the scale of 2. For each integer k, H_k and G_k are matrices with size $r \times r$. More degrees of freedom are provided by the matrix elements in these filters than a traditional scalar wavelet. The following useful properties such as orthogonality, symmetry and higher order of approximation are incorporated into the multiwavelet filters due to these extra degrees of freedom. All these properties cannot be possessed by a scalar wavelet at the same time [20].

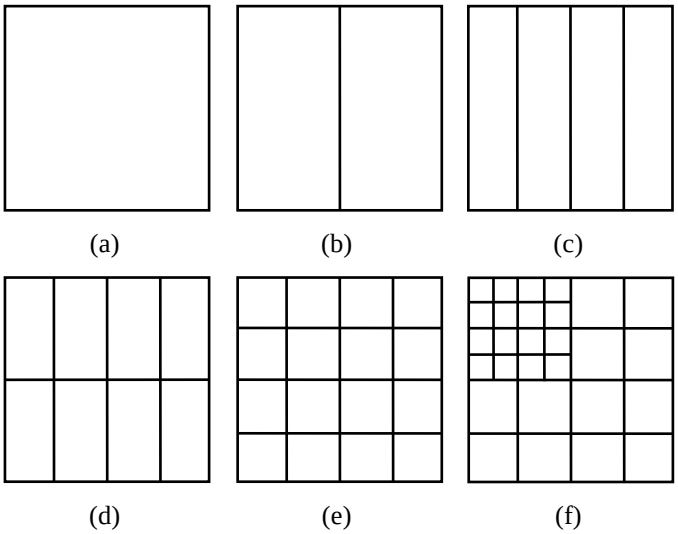

Fig.3.(a) Image (b) Prefilter along rows (c) First row decomposition (d) Prefilter along columns (e) First column and first level decomposition (f) Second level decomposition

The Fig.3 shows the different stages of two level multiwavelet decompositions. Prefiltering step is more essential when using Multiwavelet transform to produce the required multiple streams [21]. In general, multiwavelets produce $4+12K$ number of subbands, for a K^{th} level decomposition. In the first level decomposition, 16 subbands are produced as shown in Fig.4.(a). In the second level decomposition, the four 'low-low pass' subbands of the first level are further decomposed to 16 subbands. In total it produces 28 subbands as shown in Fig.4.(b) that includes high-low, low-high and high-high subbands of first level decomposition [22].

L_1L_1	L_1L_2	L_1H_1	L_1H_2
L_2L_1	L_2L_2	L_2H_1	L_2H_2
H_1L_1	H_1L_2	H_1H_1	H_1H_2
H_2L_1	H_2L_2	H_2H_1	H_1H_2

(a)

L_1L_1	L_1L_2	L_1H_1	L_1H_2	$L_1H_1^1$	$L_1H_2^1$
L_2L_1	L_2L_2	L_2H_1	L_2H_2		
H_1L_1	H_1L_2	H_1H_1	H_1H_2	$L_2H_1^1$	$L_2H_2^1$
H_2L_1	H_2L_2	H_2H_1	H_1H_2		
$H_1L_1^1$		$H_1L_2^1$		$H_1H_1^1$	$H_1H_2^1$
$H_2L_1^1$		H_2L_2		$H_2H_1^1$	$H_1H_2^1$

(b)

Fig.4.(a) Subbands of first level decomposition (b) Subbands of second level decomposition

Four main subbands with their own four subbands are obtained as the output of the combination of filters in each decomposition level. The four subbands L_1L_1, L_1L_2, L_2L_1 and L_2L_2 are considered as approximate coefficients and remaining 12 subbands are detail coefficients. In that L_1H_1, L_1H_2, L_2H_1 and L_2H_2 are horizontal, H_1L_1, H_1L_2, H_2L_1 and H_2L_2 are vertical and H_1H_1, H_1H_2, H_2H_1 and H_2H_2 are diagonal coefficients. In each level of decomposition, only the four subbands of approximate coefficients are decomposed into 16 subbands to produce the next level decomposition [23].

GHM multiwavelet is used in this work due its versatility and accuracy. In GHM, there are two low pass and high pass filters for decomposition. GHM multiwavelet has two important features i.e., orthonormality of integer translates of scaling functions and an approximation order of two [24]. GHM scaling functions have short support, orthogonality and are symmetric about their centres. Hardin-Marasovich (HM) is also used in this analysis for comparison.

After applying HM and GHM multiwavelet decomposition on the input CCA image. Energy is calculated for each subband. In an $N \times N$ subimage, energy is computed according to the following equation

$$\text{Energy} = \sum_i \sum_j x_{ij}^2 / N^2 \quad (5)$$

where, x_{ij} is the ij^{th} pixel value of the sub images. Energy is mainly concentrated in the low frequency sections after GHM multiwavelet transformation [25]. These subband energies are analysed to find if there is any correlation between CCA abnormalities and energy coefficients.

3. RESULTS AND DISCUSSION

Video of CCA with a length of 5 second is taken and converted into images at the rate of 25 frames per second. The proposed decomposition algorithm is applied on normal and abnormal CCA images using HM and GHM multiwavelets.

The Fig.5 shows the first level GHM decomposed normal and abnormal CCA images of size 512×512. The Fig.6, Fig.7 and Fig.8 show only the subbands of approximation coefficients of second, third and fourth level GHM decomposition respectively. The size of second, third and fourth level images are 256×256, 128×128 and 64×64 respectively. Decomposition is done for four levels as the information is lost beyond that. Subband energy values are calculated for all the four levels and tabulated for analysis. The energy values obtained for normal and abnormal CCA images using GHM multiwavelet are given in Table.1.

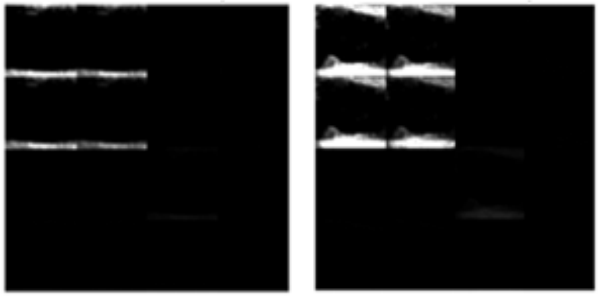

Fig.5. First level GHM decomposition of normal and abnormal images

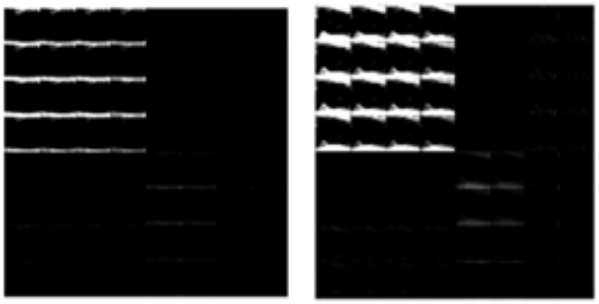

Fig.6. Second level GHM decomposition of normal and abnormal images

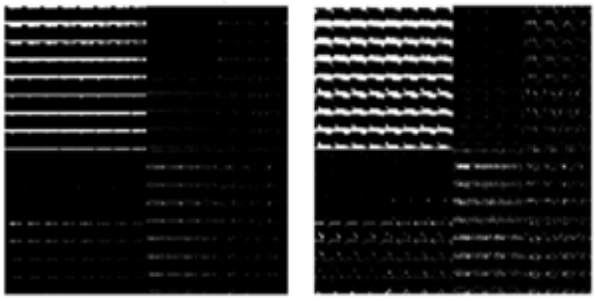

Fig.7. Third level GHM decomposition of normal and abnormal images

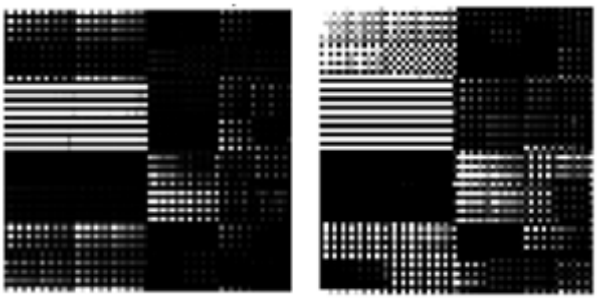

Fig.8. Fourth level GHM decomposition of normal and abnormal images

Table.1. Subband Energy coefficients of normal and abnormal CCA images using GHM multiwavelet decomposition

Sub band	Normal image				Abnormal image			
	Level 1 ($x10^4$)	Level 2 ($x10^4$)	Level 3 ($x10^4$)	Level 4 ($x10^4$)	Level 1 ($x10^4$)	Level 2 ($x10^4$)	Level 3 ($x10^4$)	Level 4 ($x10^4$)
Ea1	0.52453	1.9183	3.4689	0.516	4.1008	15.22	54.755	12.94
Ea2	0.22663	0.8388	1.6236	0.554	1.7721	6.619	24.455	10.41
Ea3	0.23089	0.9545	7.0328	18.441	1.7892	6.898	25.437	209.43
Ea4	0.09976	0.4175	2.8890	12.228	0.7732	3.009	11.043	94.64
Eh1	0.02156	0.0821	0.1799	0.078	0.1675	0.636	2.435	2.23
Eh2	0.00007	0.0011	0.0234	0.037	0.0005	0.011	0.153	0.53
Eh3	0.00949	0.0411	0.3436	1.703	0.0731	0.289	1.193	11.75
Eh4	0.00003	0.0005	0.0247	0.233	0.0002	0.006	0.127	3.61
Ev1	0.02530	0.1273	0.5811	17.141	0.1816	0.811	4.141	74.99
Ev2	0.01094	0.0557	0.2509	9.611	0.0785	0.353	1.898	30.94
Ev3	0.00080	0.0113	0.6384	0.672	0.0038	0.063	1.908	4.77
Ev4	0.00034	0.0050	0.3474	0.687	0.0016	0.028	1.025	10.21
Ed1	0.00001	0.0056	0.0081	0.0835	0.0001	0.034	0.174	3.12
Ed2	0.00001	0.0001	0.0069	0.0177	0.0001	0.001	0.069	1.21
Ed3	0.00003	0.0005	0.0305	0.0099	0.0002	0.003	0.168	0.73
Ed4	0.00001	0.0001	0.0091	0.0055	0.0001	0.001	0.099	0.65

Ea1, Ea2, Ea3 and Ea4 are energy values of four subbands of the approximation coefficients. Eh1, Eh2, Eh3 and Eh4 are the four subband energies of Horizontal coefficients. Subband energy of vertical and diagonal coefficients are given as Ev1, Ev2, Ev3, Ev4 and Ed1, Ed2, Ed3, Ed4 respectively. From Table.1, it is observed that the energy is mainly concentrated in the low frequency bands i.e. approximation coefficients. Energy level of each subband obtained from normal and abnormal images using HM and GHM multiwavelet is plotted and analysed for all the four levels of decomposition. The Fig.9 and Fig.10 show the energy plots of first and second level HM and GHM subbands energy coefficients of normal and abnormal images respectively. Subbands of normal image are shown in white bars and the subbands of abnormal images are shown in black bars in the energy level diagram.

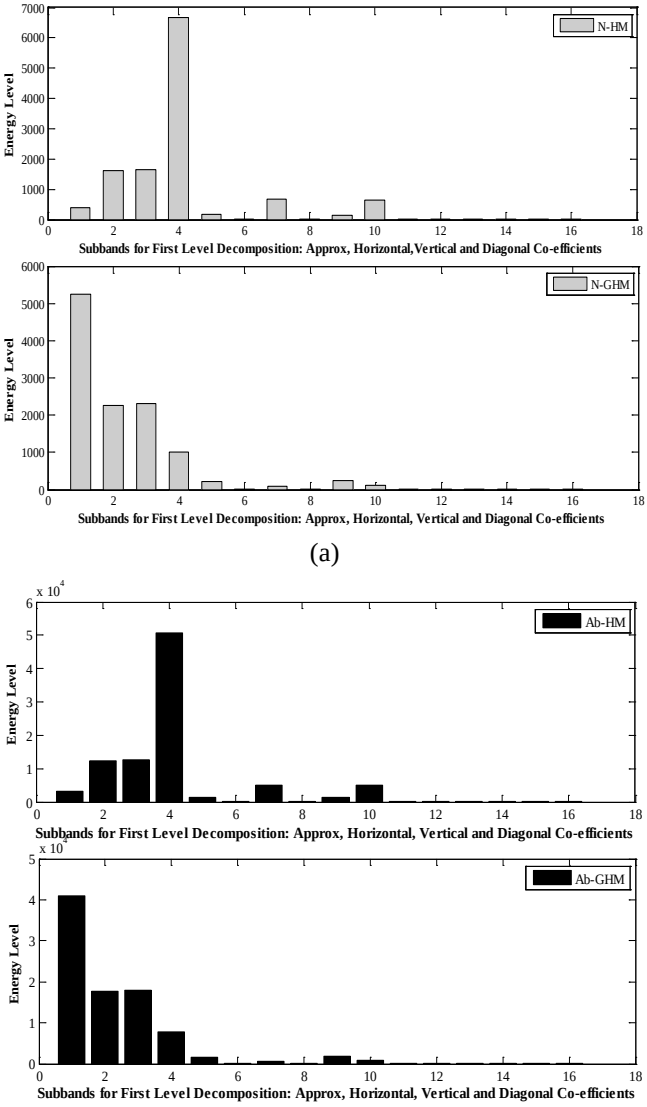

(a)

(b)

Fig.9. Subband energy comparison of normal and abnormal CCA images for HM and GHM multiwavelet first level decomposition

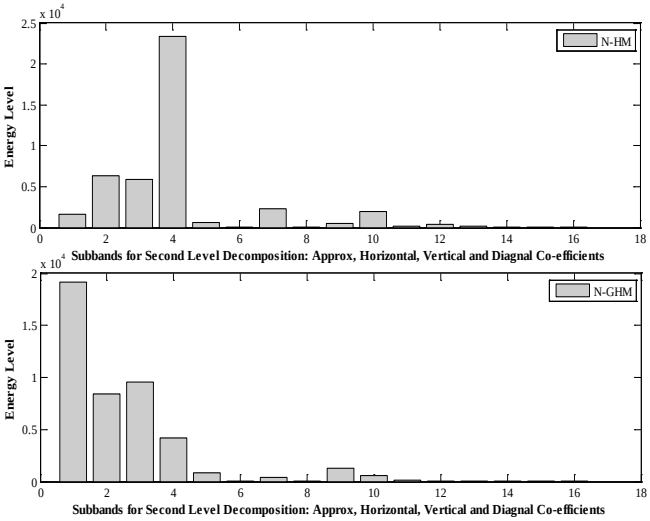

(a)

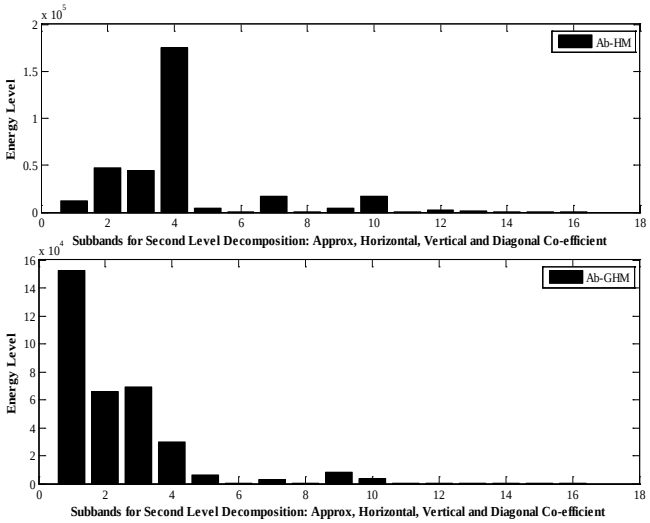

(b)

Fig.10. Subband energy comparison of normal and abnormal CCA images for HM and GHM multiwavelet second level decomposition

By analysing the variations in the energy values of subbands of normal and abnormal decomposed CCA image, it is found that the diagonal energy coefficients have very little amount of energy in all the levels of decomposition. The horizontal and vertical energy coefficients have small amount of energy. But most of the energy is preserved in the approximate coefficients and it increases for every level of decomposition. Plots clearly show that the energy values vary for normal and abnormal image in all the levels. The energy values of subbands given in the Table.1 are for a normal and abnormal subject. Multiwavelets preserve high frequency information in the image i.e edges and give very good performance at the boundaries. As the formation of plaque is in the inner walls of the artery and alters the boundary, the difference between the normal and abnormal CCA is expected to reflect in the subband energy values of diagonal coefficients. While comparing the energy values of normal and abnormal CCA image given in Table.1, the same is observed. The energy values of diagonal coefficients of normal and abnormal images differ largely. Hence these values are further used for classification. They can be used to develop classifiers to classify the normal and abnormal CCA.

4. CONCLUSION

A method is proposed to analyze the abnormalities in longitudinal B-mode ultrasound common carotid artery images using HM and GHM multiwavelets. Normal and abnormal CCA image are taken and decomposed up to four levels. The energy value of each subband is calculated, plotted and analyzed for all the four levels of decomposition. It is found that most of the energy is concentrated in approximate coefficients and a small amount of energy is present in horizontal and vertical coefficients. The energy values obtained from normal images are compared with the energy values obtained from abnormal images. It is observed that the energy values have large difference for normal and abnormal images. Hence, it is concluded that the subband energy can be used as a feature for the diagnosis of abnormalities in CCA. Atherosclerosis and CVDs are highly correlated to the risk factors such as cholesterol, blood pressure, smoking and diabetics. Future work will focus on considering all these risk factors to validate the good features to detect abnormalities in the common carotid artery. Further testing of the proposed method has to be done in a larger image dataset to classify the healthy and unhealthy subjects.

ACKNOWLEDGMENT

The authors are grateful to All India Council for Technical Education (AICTE), India for funding this project under Research Promotion Scheme (RPS). The authors would like to thank Dr. Suresh from Mediscan systems, Chennai, India and Dr. Kandasamy from Sudha Hospital, Erode, India for having kindly provided the inputs for this work.

REFERENCES

[1] Abigail Swillens, Gianluca De Santis, Joris Degroote, Lasse Lovstakken, Jan Vierendeels and Patrick Segers, “Accuracy of Carotid Strain Estimates From Ultrasonic Wall Tracking: A Study Based on Multiphysics Simulations and In Vivo Data”, *IEEE Transactions on Medical Imaging*, Vol. 31, No. 1, pp. 131-139, 2012.

[2] Efthyvoulos C. Kyriacou et al.,“A Review of Noninvasive Ultrasound Image Processing Methods in the Analysis of Carotid Plaque Morphology for the Assessment of Stroke Risk”, *IEEE Transactions on Information Technology in Biomedicine*, Vol. 14, No. 4, pp. 1027-1038, 2010.

[3] David C. Wang, Roberta Klatzky, Bing Wu, Gregory Weller, Allan R. Sampson and George D. Stetten, “Fully Automated Common Carotid Artery and Internal Jugular Vein Identification and Tracking Using B-Mode Ultrasound”, *IEEE Transactions on Biomedical Engineering*, Vol. 56, No. 6, pp. 1691-1699, 2009.

[4] Jianwen Luo, Ronny X. Li and Elisa E. Konofagou, “Pluse Wave Imaging of the Human Carotid Artery: An In Vivo Feasibility Study”, *IEEE Transactions on Ultrasonics, Ferroelectrics, and Frequency Control*, Vol. 59, No. 1, pp. 174-181, 2012.

[5] Toufik Zakaria, Zhao Qin and Roch Listz Maurice, “Optical-Flow-based B-Model Elastography: Application in the Hypertensive Rat Carotid”, *IEEE Transactions on Medical Imaging*, Vol. 29, No. 2, pp. 570-578, 2010.

[6] Filippo et al., “Hypothesis Validation of Far- Wall Brightness in Carotid-Artery Ultrasound for Feature-based IMT Measurement using a Combination of Level-Set Segmentation and Registration”, *IEEE Transactions on Instrumentation and Measurement*, Vol. 61, No. 4, pp. 1054-1063, 2012.

[7] C.P. Loizou, V. Murray, M.S. Pattichis, M. Pantziaris and C.S. Pattichis, “Multiscale Amplitude-Modulation Frequency-Modulation (Am-Fm) Texture Analysis of Ultrasound Images of the Intima and Media Layers of the Carotid Artery”, *IEEE Transactions on Information Technology in Biomedicine*, Vol. 15, No. 2, pp. 178-188, 2011.

[8] Francois Destrempes, Jean Meunier, Marie-France Giroux, Gilles Soulez and Guy Cloutier, “Segmentation of Plaques

in Sequences of Ultrasonic B-Mode Images of Carotid Arteries Based on Motion Estimation and a Bayesian Model", *IEEE Transactions on Biomedical Engineering*, Vol. 58, No. 8, pp. 2202-2211, 2011.

[9] D.C. Barratt, B.B. Ariff, K.N. Humphries, S.A. Mc.G. Thom and A.D. Hughes, "Reconstruction and Quantification of the Carotid Artery Bifurcation from 3-D Ultrasound Images", *IEEE Transactions on Medical Imaging*, Vol. 23, No. 5, pp. 567-583, 2004.

[10] M. Larsson, F. Kremer, P. Claus, T. Kuznetsova, L.A. Brodin and J. Dhooge, "Ultrasound-Based Radial and Longitudinal Strain Estimation of the Carotid Artery: A Feasibility Study", *IEEE Transactions on Ultrasonics, Ferroelectrics and Frequency Control*, Vol. 58, No. 10, pp. 2244-2251, 2011.

[11] Nikolaos N. Tsiaparas, Spyretta Golemati, Ioannis Andreadis, John S. Stoitsis, Ioannis Valavanis and Konstantina S. Nikita, "Comparison of Multiresolution Features for Texture Classification of Carotid Atherosclerosis From B-Mode Ultrasound", *IEEE Transactions on Information Technology in Biomedicine*, Vol. 15, No. 1, pp. 130-137, , 2011.

[12] Jayanthi K. Balasundaram and R.S.D. Wahida Banu, "Carotid Artery Boundary Extraction for the Analysis of Cardiovascular Diseases", *International Journal of Medical Engineering and Informatics*, Vol. 1, No. 3, pp. 290-297, 2009.

[13] Jayanthi K. Balasundaram and R.S.D. Wahida Banu, "A Non-Invasive Study of Alterations of the Carotid Artery with Age using Ultrasound Images", *Medical and Biological Engineering and Computing*, Vol. 44, No. 9, pp. 767-772, 2006.

[14] Hamid Soltanian-Zadeh, Farshid Rafiee-Rad and D. Siamak Pourabdollah-Nejad, "Comparison of Multiwavelet, Wavelet, Haralick, and Shape Features for Microcalcification Classification in Mammograms", *Pattern Recognition*, Vol. 37, No. 10, pp. 1973-1986, 2004.

[15] S. Ramakrishnan and S. Selvan, "Multiwavelets Domain Singular Value Features for Image Texture Classification", *Journal of Zhejiang University-Science A*, Vol. 8, No. 4, pp. 538-549, 2007.

[16] Manju Mathew, A.B. Premkumar and A.S. Madhukumar, "Spectrum-Efficient Cognitive Radio Transceiver using Multiwavelet Filters", *International Scholarly Research Network*, Vol. 2012, pp. 1-13, 2012.

[17] Padmanabhareddy Vundela and Varadarajan Sourirajan, "A Robust Multiwavelet-based Watermarking Scheme for Copyright Protection of Digital Images using Human Visual System", *International Arab Journal of Information Technology*, Vol. 10, No. 6, pp. 4128-4228, 2011.

[18] Jing-Wein Wang, "Evolutionary Optimization Approach for Fingerprint Classification", *Proceedings of the World Congress on Engineering*, Vol. 2, pp. 1-5, 2011.

[19] Chin-Pan Huang and Ching-Chung Li, "Secret Image Sharing using Multiwavelet Transform", *Journal of Information Science and Engineering*, Vol. 27, No. 2, pp. 733-748, 2011.

[20] Ali Zifa, Mohammed Hassan Moradi and Shahriar Gharibzadeh, "Microarray Image Enhancement by Denoising using Decimated and Undecimated Multiwavelet Transforms", *Signal, Image and Video Processing*, Vol. 4, No. 2, pp. 177-185, 2010.

[21] Ivan W. Selesnick, "Multiwavelet bases with Extra Approximation Properties", *IEEE Transactions on Signal Processing*, Vol. 46, No. 11, pp. 2898-2908, 1998.

[22] N. Leelavathy, V. Prasade, S. Srinivas Kumar et al., "Oblivious Image Watermarking in Discrete Multiwavelet Domain using QIMM", *Journal of Multimedia*, Vol. 6, No. 4, pp. 359-368, 2011.

[23] U.S. Ragupathy, D. Baskar and A. Tamilarasi, "A Novel Method of Image Compression using Multiwavelets and Set Partitioning Algorithm", *Proceedings of 3rd International Conference on Industrial and Information System*, pp. 1-6, 2009.

[24] Chihang Zhao, Yongsheng Gao, Jie He and Jie Lianl, "Recognition of Driving Postures by Multiwavelet Transform and Multilayer Perceptron Classifier", *Engineering Applications of Artificial Intelligence*, Vol. 25, No. 8, pp. 1677-1686, 2012.

[25] Yuanning Liu, Fei He, Yonghua Zhao and Ning Wang, "An Iris Recognition based on GHM Multi-Wavelet Transformation", *Proceedings of 4th International Conference on Innovative Computing, Information and Control*, pp. 793-796, 2009.